Earth and Planetary Science Letters 594 (2022) 117716

Contents lists available at ScienceDirect

Earth and Planetary Science Letters

www.elsevier.com/locate/epsl

Moderate levels of oxygenation during the late stage of Earth's Great Oxidation Event

Frantz Ossa Ossa [a,b,c,*], Jorge E. Spangenberg [d], Andrey Bekker [e,c], Stephan König [a,f], Eva E. Stüeken [g], Axel Hofmann [c], Simon W. Poulton [h], Aierken Yierpan [a], Maria I. Varas-Reus [a], Benjamin Eickmann [a], Morten B. Andersen [b], Ronny Schoenberg [a,c]

[a] Department of Geosciences, University of Tuebingen, 72074 Tuebingen, Germany
[b] School of Earth & Environmental Sciences, Cardiff University, Cardiff CF10 3AT, UK
[c] Department of Geology, University of Johannesburg, 2092 Johannesburg, South Africa
[d] Institute of Earth Surface Dynamics (IDYST), University of Lausanne, 1015 Lausanne, Switzerland
[e] Department of Earth and Planetary Sciences, University of California, Riverside, CA 92521, USA
[f] Instituto Andaluz de Ciencias de la Tierra (IACT), Consejo Superior de Investigaciones Científicas and Universidad de Granada, Avenida las Palmeras 4, Armilla, 18100 Granada, Spain
[g] School of Earth & Environmental Sciences, University of St. Andrews, St. Andrews, KY16 9AL, UK
[h] School of Earth and Environment, University of Leeds, Leeds LS2 9JT, UK

ARTICLE INFO

Article history:
Received 20 January 2022
Received in revised form 26 June 2022
Accepted 4 July 2022
Available online xxxx
Editor: B. Wing

Keywords:
Paleoproterozoic
Lomagundi carbon isotope excursion
Great Oxidation Event
Francevillian Group
biogeochemical cycles

ABSTRACT

The later stages of Earth's transition to a permanently oxygenated atmosphere during the Great Oxidation Event (GOE; ~2.43–2.06 Ga) is commonly linked with the suggestion of an "oxygen overshoot" during the ~2.22–2.06 Ga Lomagundi Event (LE), which represents Earth's most pronounced and longest-lived positive carbon isotope excursion. However, the magnitude and extent of atmosphere-ocean oxygenation and implications for the biosphere during this critical period in Earth's history remain poorly constrained. Here, we present nitrogen (N), selenium (Se), and carbon (C) isotope data, as well as bio-essential element concentrations, for Paleoproterozoic marine shales deposited during the LE. The data provide evidence for a highly productive and well-oxygenated photic zone, with both inner and outer-shelf marine environments characterized by nitrate- and Se oxyanion-replete conditions. However, the redoxcline subsequently encroached back onto the inner shelf during global-scale deoxygenation of the atmosphere-ocean system at the end of the LE, leading to locally enhanced water column denitrification and quantitative reduction of selenium oxyanions. We propose that nitrate-replete conditions associated with fully oxygenated continental shelf settings were a common feature during the LE, but nitrification was not sufficiently widespread for the aerobic nitrogen cycle to impact the isotopic composition of the global ocean N inventory. Placed in the context of Earth's broader oxygenation history, our findings indicate that O_2 levels in the atmosphere-ocean system were likely much lower than modern concentrations. Early Paleoproterozoic biogeochemical cycles were thus far less advanced than after Neoproterozoic oxygenation.

1. Introduction

Biological evolution and ecosystem complexity are intimately linked to the magnitude and expansion of Earth's surface oxygenation through time. Constraining the timing at which the atmosphere-hydrosphere system became significantly oxygenated, reaching near-modern levels, may help to shed new light on the emergence and proliferation of O_2-dependent life, including complex life forms such as eukaryotes. Geochemical evidence based on multiple sulfur isotope systematics suggests a first transient rise in atmospheric O_2 concentration to above 10^{-6} of the present atmospheric level (PAL) during the initial stages of the Great Oxidation Event (GOE) at ~2.43–2.32 Ga (Bekker et al., 2004; Catling and Zahnle, 2020; Farquhar et al., 2000; Hannah et al., 2003; Holland, 2006; Warke et al., 2020). In particular, the disappearance of mass-independent fractionation of sulfur isotopes and redox-sensitive detrital minerals (e.g., uraninite, pyrite) from sedimentary records, followed by the appearance of red beds, are some of the most im-

* Corresponding author at: School of Earth & Environmental Sciences, Cardiff University, Cardiff CF10 3AT, UK.
E-mail address: frantz.ossaossa@gmail.com (F. Ossa Ossa).

https://doi.org/10.1016/j.epsl.2022.117716

portant markers for the GOE (Bekker et al., 2004; Farquhar et al., 2000; Holland, 2006; Lyons et al., 2014). However, the permanent rise of atmospheric O_2 likely occurred in the second half of the GOE, during the ~2.22–2.06 Ga Lomagundi Event (LE) (Poulton et al., 2021). The LE represents the most pronounced and longest-lived positive carbon isotope excursion in Earth history (Bekker, 2022; Karhu and Holland, 1996), and is considered to have resulted in transient highly elevated levels of O_2, but to an extent that is currently unclear (Bekker and Holland, 2012). Atmospheric O_2 concentrations are estimated to have been at levels below 1% (Colwyn et al., 2019) to as high as ~10% PAL (Holland, 2006; Kanzaki and Murakami, 2016) throughout most of the subsequent Proterozoic, up until the ~750–539 Ma Neoproterozoic Oxygenation Event (NOE), when atmospheric O_2 is commonly considered to have increased further (Holland, 2006; Lyons et al., 2014; Colwyn et al., 2019).

The Paleoproterozoic ocean is widely considered to have been redox-stratified during the GOE (Alcott et al., 2019; Asael et al., 2018; Cheng et al., 2019; Holland, 2006; Kipp et al., 2017, 2018; Lyons et al., 2014; Poulton et al., 2021; Stüeken et al., 2016), with a redoxcline situated above storm wave-base and with O_2 concentrations in surface waters that may have been above 0.4 to 1 μM (Hardisty et al., 2014; Kipp et al., 2017). The post-GOE ocean likely remained redox stratified (Poulton et al., 2010; Poulton and Canfield, 2011; Ossa Ossa et al., 2018; Planavsky et al., 2011; Scott et al., 2008), until episodic oxygenation of the deeper ocean occurred during the NOE (Alcott et al., 2019; Canfield et al., 2007; Lenton et al., 2014; von Strandmann et al., 2015).

Mainly based on carbon isotope systematics, the LE is generally considered to reflect a combination of high rates of primary productivity and increased organic carbon burial (Bekker, 2022; Bekker and Holland, 2012; Husson and Peters, 2017; Karhu and Holland, 1996). Elevated organic productivity may have been initiated by a high phosphorus flux to the oceans, potentially due to leaching of terrestrial rocks by sulfuric acid generated through oxidative weathering of pyrite (Bekker and Holland, 2012; Konhauser et al., 2011). The rate of organic matter burial exceeded the rate of its reoxidation, allowing the release of marine photosynthetic O_2 which likely caused an atmospheric O_2 overshoot (Bekker and Holland, 2012). However, redox and biogeochemical proxies used for constraining O_2 concentrations in the atmosphere-ocean system during the LE have yielded contrasting estimates (Blättler et al., 2018; Colwyn et al., 2019; Hardisty et al., 2014; Holland, 2006; Kanzaki and Murakami, 2016; Kipp et al., 2017; Mänd et al., 2020). For example, estimates based on the chemical and Cr isotope compositions of Paleoproterozoic paleosols suggest that atmospheric O_2 levels remained lower than 1–10% PAL (Colwyn et al., 2019; Kanzaki and Murakami, 2016). By contrast, thick (~800 m) evaporite deposits supposedly deposited in marginal-marine environments during the LE, which are interpreted to reflect the oceanic sulfate inventory, as well as associated S, Ca, Sr and O isotope compositions, have been proposed to reflect an oxygenated atmosphere-ocean system with higher than 20% of the modern atmosphere-ocean oxidizing capacity (Blättler et al., 2018).

Although the mechanism that caused the end of the LE is still debated, its termination, based on C, S, Fe, V, Mo, U and Se biogeochemical proxies in marine sediments, is viewed to be contemporaneous with a drop in O_2 levels in the atmosphere-ocean system (Asael et al., 2018; Canfield et al., 2013; Kipp et al., 2017; Kump et al., 2011; Lyons et al., 2014; Ossa Ossa et al., 2018, 2021a; Planavsky et al., 2012; Scott et al., 2014). However, based on U and Cr isotope compositions and trace-metal (Mo, Cr, U and Re) enrichments in mid-Paleoproterozoic shales from the Zaonega Formation, northwestern Russia, it has been proposed that the atmosphere-ocean system was still well-oxygenated millions of years after the termination of the LE (Mänd et al., 2020, 2022). Since the biogeochemical cycling of S, Fe, V, Mo and U yield stable oxyanions at circumneutral pH in marine environments at relatively low redox potential (i.e., Eh $<$ 0 V; Rue et al., 1997; Stumm and Morgan, 1970), they are only sensitive as redox indicators at very low levels of environmental O_2 (e.g., Andersen et al., 2020; Dang et al., 2022). Furthermore, a wide range of redox and non-redox processes can significantly fractionate Cr isotopes, regardless of the level of O_2 available in the environment (e.g., Babechuk et al., 2017, 2018; Miletto et al., 2021). Clearly, further constraints are needed given current uncertainties in estimates of environmental O_2 availability. Marine proxies that are redox-sensitive at a higher oxygen threshold (i.e., Eh $\gg$ 0 V) at circumneutral pH are thus required to shed light on the potential for higher oxygenation levels during the LE.

To provide new insight into the evolution of oceanic redox structure during and after the LE and links to environmental oxygenation, we present combined nitrogen and selenium isotope ratios, together with new Fe speciation and organic carbon isotope data, for well-preserved black shales from the mid-Paleoproterozoic Francevillian Group (Gauthier-Lafaye and Weber, 2003; Ossa Ossa et al., 2018, 2021a), which we compare with other LE sedimentary successions. These isotopic systems allow us to track the marine biogeochemical cycles of nitrogen and selenium in redox-stratified basins (Ader et al., 2016; Rue et al., 1997; Sigman and Fripiat, 2019; Stüeken, 2017; Stüeken et al., 2016), as well as the behavior of nitrate (NO_3^-) and selenate (SeO_4^{2-}), both of which are stable at much higher redox thresholds than SO_4^{2-}, MoO_4^{2-}, Fe^{3+} and U^{6+} (Rue et al., 1997; Stumm and Morgan, 1970). Both nitrate and selenate are stable at Eh $>$ 0.4 V at circumneutral pH, and only build up to significant levels in open-marine environments if the water column is well oxygenated (Rue et al., 1997). Tracing the biogeochemical nitrogen cycle is complicated, because the nitrogen isotope composition of sedimentary rocks can be influenced by a wide range of both biotic and abiotic processes (Ader et al., 2016; Sigman and Fripiat, 2019; Stüeken et al., 2016). However, when paired with the Se biogeochemical cycle, a more rigorous constraint may be achieved, whereby the behavior of NO_3^- and SeO_4^{2-} is expected to be internally consistent under oxic, suboxic and anoxic conditions, and this consistency should be recorded in the isotopic signatures. Combined N and Se isotope analyses thus provide a powerful opportunity to unravel the magnitude and extent of ocean oxygenation during and shortly after the LE.

2. Geological setting

The Francevillian Group is an unmetamorphosed ~2.1 Ga Paleoproterozoic sedimentary succession, characterized by well-preserved smectite-rich clay minerals in black shales (see Supplementary Information SI 1 for the preservation of Francevillian Group samples studied here), in southeast Gabon (Gauthier-Lafaye and Weber, 2003; Ossa Ossa et al., 2013, 2018), developed within the ~44,000 km^2 Francevillian basin (Fig. 1A). The Francevillian basin is subdivided into four sub-basins including the Booué (Plateau des Abeilles), Lastoursville, Franceville and Okindja (Fig. 1A). The Francevillian Group was deposited during the peak and end of the ~2.22–2.06 Ga LE (Bros et al., 1992; Horie et al., 2005; Ossa Ossa et al., 2013, 2018, 2021a; Préat et al., 2011) and is subdivided into five formations from the Francevillian A (FA) at the bottom to FE at the top (Fig. 1B; Gauthier-Lafaye and Weber, 2003). Our study focuses on carbonaceous, fine-grained sedimentary rocks spanning the FB to FC formations. These units were deposited in open to marginal marine settings (see Supporting Information SI 1 for detailed sedimentological description) during the peak and fall of the LE (Ossa Ossa et al., 2013, 2018; Préat et al., 2011). Besides sedimentological constraints, a high rate of manganese oxidation associated with moderate iron enrichment in an

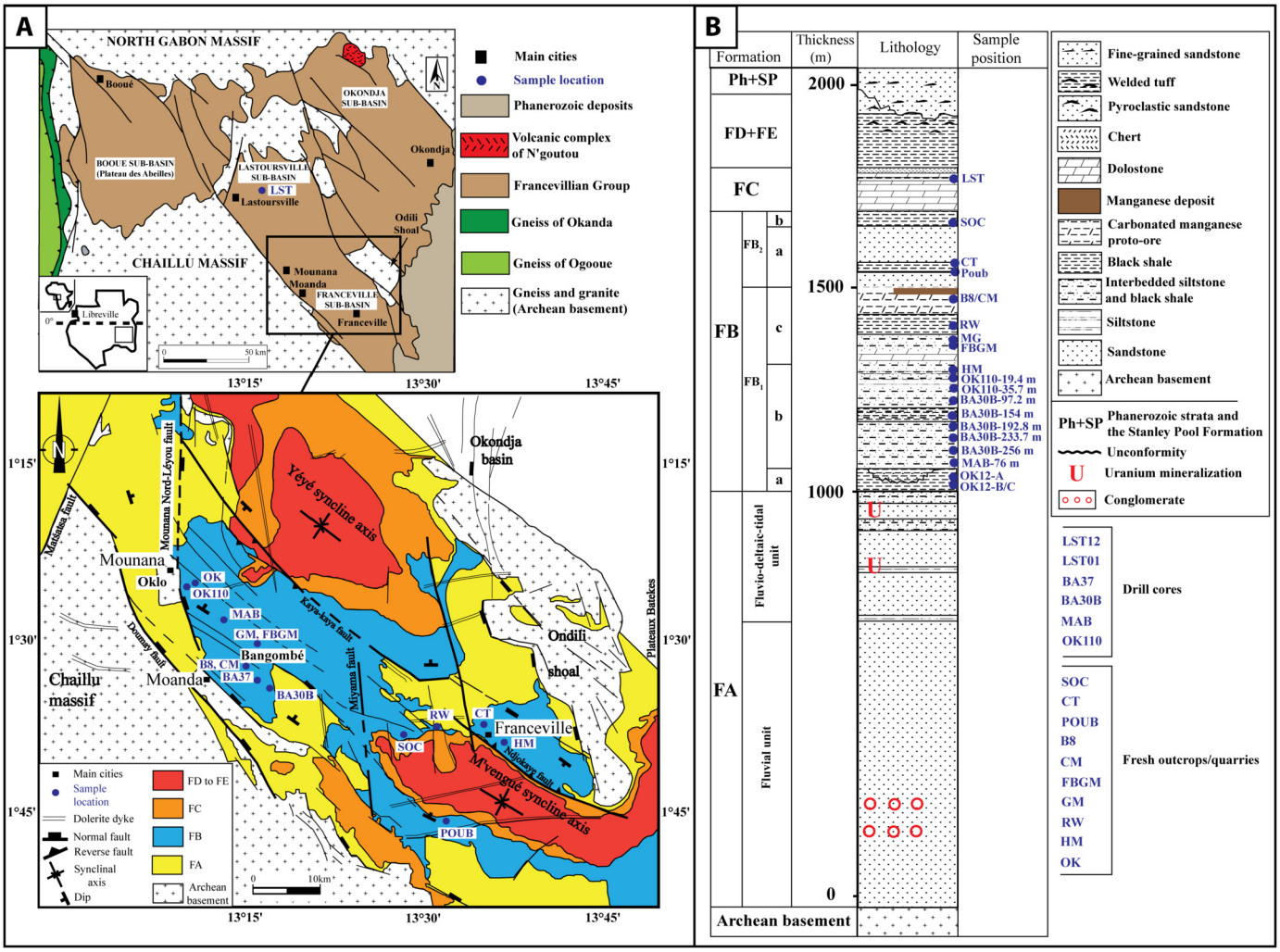

Fig. 1. (A) Simplified geological map of the Francevillian basin and sample locations. (B) Lithostratigraphic column of the Francevillian Group showing stratigraphic position of samples (modified from Gauthier-Lafaye and Weber, 2003; Ossa Ossa et al., 2013, 2018, 2021a; Préat et al., 2011).

upwelling zone (Canfield et al., 2013; Gauthier-Lafaye and Weber, 2003; Ossa Ossa et al., 2018), as well as elevated V/Al ratios (Canfield et al., 2013; Ossa Ossa et al., 2021a), provide support that the Francevillian basin was well connected to the open ocean during deposition of the FB and FC formations.

3. Methods

3.1. Major elements

Powdered samples were analysed for major element concentrations by X-ray fluorescence spectroscopy. Analyses were carried out on fusion beads, using a PANalytical MagiX Pro PW2540 spectrometer at the University of Johannesburg. Accuracy was checked with certified reference materials and was better than 1%. Elemental concentrations are reported in wt.% with a detection limit of 0.004 wt.%.

3.2. Iron speciation analysis

Iron speciation analyses was performed at the University of Leeds, UK using a calibrated sequential extraction protocol followed by Fe analysis via AAS (Poulton et al., 2021; Poulton and Canfield, 2005). This method is designed to operationally quantify four different pools of Fe considered to be highly-reactive (Fe_{HR}) towards sulfide in surface and near-surface environments: (*a*) pyrite S extracted via Cr-reduction followed by trapping as Ag_2S, with Fe calculated assuming an FeS_2 stoichiometry (Fe_{Py}); (*b*) carbonate-associated iron extracted with a sodium acetate solution (Fe_{Carb}); (*c*) ferric oxides extracted with a dithionite solution (Fe_{Ox}); and (*d*) mixed-valence iron oxides, principally magnetite, extracted using ammonium oxalate (Fe_{Mag}). The total iron content in ancient marine shales (Fe_T) represents the sum of Fe_{HR} and Fe bound in silicates (Poulton et al., 2021; Poulton and Canfield, 2005). Samples were run alongside an international Fe speciation standard (WHIT; Alcott et al., 2020), with replicate analyses giving a RSD of <5% for all Fe pools. For a detailed description of the interpretation of Fe speciation data, see Supplementary Information SI 2.

3.3. Carbon and nitrogen isotope analyses

The carbon and nitrogen stable isotope composition of bulk rock ($\delta^{13}C_{org}$ and $\delta^{13}C_{bulk}$, respectively) and the nitrogen isotope composition of the separated kerogen ($\delta^{15}N_{ker}$) were determined by elemental analysis/isotope ratio mass spectrometry (EA/IRMS; Flash EA coupled to a Thermo Scientific Delta V isotope ratio mass spectrometer via a Conflow III interface) at the Institute of Earth Surface Dynamics, University of Lausanne (IDYST-UNIL). Kerogen, the fraction of organic matter insoluble in organic solvents, was separated from powdered shale samples using non-oxidizing acids (HCl, HF) to dissolve the mineral matrix. For $\delta^{13}C$

and $\delta^{15}N$ analyses, separate EA combustions were performed using sample aliquots with a 1:50 weight size difference. The isotope ratios are expressed in conventional delta (δ) notation as the per mil (‰) of $^{13}C/^{12}C$ and $^{15}N/^{14}N$ of the sample relative to the standard VPDB for $\delta^{13}C$ and Air-N_2 for $\delta^{15}N$. The measured isotopic ratios were converted to the international scales with a 3- or 4-point calibration using international reference materials (IRMs; USGS-24, USGS-40, USGS-41, IAEA-600 or USGS64, USGS65, and USGS66) and inhouse standards. The accuracy and precision of the analyses were checked periodically through the analysis of standards not included as calibration standards. Separate aliquots of the USGS SGR-1b standard (petroleum and carbonate-rich shale) were decarbonated and analysed for $\delta^{13}C$ and $\delta^{15}N$ values. The obtained values ($\delta^{13}C = -29.29 \pm 0.17$‰, V-PDB; $n = 10$; $\delta^{15}N = 17.45 \pm 0.26$‰, Air-$N_2$; $n = 6$) are in good agreement with the values reported by Dennen et al. (2006) for SGR-1 ($\delta^{13}C = -29.3 \pm 0.3$‰, $n = 27$; $\delta^{15}N = 17.4 \pm 0.9$‰, $n = 18$). For a detailed description of the analytical procedures, see Supplementary Information SI 2.

3.4. Selenium isotope and elemental analyses

Sample preparation and analysis was carried out at the University of Tuebingen, Germany. Selenium isotope composition was determined by the double-spike method using a ThermoFisher Scientific NeptunePlus multicollector inductively coupled plasma mass spectrometer (MC–ICP–MS) coupled with an HGX-200 hydride generator (Kurzawa et al., 2017). Data are reported in $\delta^{82/76}Se$ notation, that is, the per mil (‰) variation of $^{82}Se/^{76}Se$ relative to the NIST SRM 3149 standard. The accuracy and measurement precision were checked by analysing interlaboratory standard MH 495, international rock reference materials and for sulfide analyses in particular by repeated digestion of the Phanerozoic Navajún pyrite (König et al., 2019; Kurzawa et al., 2017). The MH 495 measured during the course of this study yielded a mean $\delta^{82/76}Se$ value of -3.24 ± 0.05‰ (2 SD, $n = 28$), which is consistent with previously reported data, while the in-house reference Navajún pyrite (König et al., 2019 and references therein) yielded a mean $\delta^{82/76}Se$ value of -2.45 ± 0.10‰ (2 SD, $n = 4$), which is within the external reproducibility as derived from multiple analytical sessions over 16 months, with a mean $\delta^{82/76}Se$ value of -2.65 ± 0.20‰ (2 SD, $n = 15$). For a detailed description of the analytical procedures, see Supplementary Information SI 2.

4. Results

The description of the main results (Tables S1, S2) is organized with respect to previous characterization of redox conditions coupled to major upwelling and/or transgression events during deposition of the FB Formation and FC_1 Member (Figs. 1B, 2, S2B; Canfield et al., 2013; Ossa Ossa et al., 2018). For example, published iron speciation data based on highly reactive (Fe_{HR}) to total Fe (Fe_T) ratios indicate that deposition of the lower FB Formation occurred in a well-oxygenated marine environment ($Fe_{HR}/Fe_T < 0.22$), which subsequently evolved to a suboxic and even euxinic (anoxic and sulfidic; denoted by $Fe_{HR}/Fe_T > 0.38$ and pyrite Fe (Fe_{Py}) to Fe_{HR} ratios > 0.7) water column setting during deposition of the upper part of the FB_{1c} unit (Figs. 2, S2B; Canfield et al., 2013; Ossa Ossa et al., 2013, 2018). Oxic conditions during deposition of most of the FB Formation, with suboxic conditions during deposition of the upper part of the FB_{1c} unit, are further supported by V/Al ratios averaging 7.7 ppm/wt.%, Mo/Al ratios averaging 0.2 ppm/wt.% and U/Al ratios averaging 7.7 ppm/wt.%, which are typical for marine black shale deposited under oxic conditions (Ossa Ossa et al., 2021a). By contrast, higher ratios of V/Al averaging 46.5 ppm/wt.%, Mo/Al averaging 1.6 ppm/wt.%, and U/Al averaging 1.2 ppm/wt.% in the Upper FC_1 Member and FD Formation indicate enhanced seawater euxinia during deposition of the upper part of the Francevillian Group (Canfield et al., 2013; Ossa Ossa et al., 2021a). This is further supported by Fe speciation data, with $Fe_{HR}/Fe_T > 0.38$ and $Fe_{Py}/Fe_{HR} > 0.7$ in the FD Formation (Canfield et al., 2013; Fig. S2).

In the lower part of the FB Formation (Fig. 2; Table S2), black shales of the FB_{1a} unit, which record the main transgressive event in the basin (Canfield et al., 2013; Gauthier-Lafaye and Weber, 2003; Ossa Ossa et al., 2013; Weber, 1968), are characterized by Se concentrations between 2 and 6 µg/g, with slightly negative $\delta^{82}Se$ values between −0.35 and −0.28‰ (mean value of −0.32‰). The $\delta^{15}N$ values of bulk samples ($\delta^{15}N_{bulk}$) and extracted kerogen ($\delta^{15}N_{ker}$) show no systematic offset and are positive, with values between +4.4 and +8.1‰ (mean value of +6.2‰). The total organic carbon (TOC) content of this sedimentary unit is high, between 3.5 and 8.8 wt.%, with $\delta^{13}C_{TOC}$ values (expressed in ‰ relative to VPDB) between −25.9 and −23.7‰ (mean value of −24.6‰).

From the FB_{1b} unit to the middle part of the FB_{1c} units (Fig. 2; Table S2), black shales have Se concentrations of 1 to 7 µg/g and predominantly negative $\delta^{82}Se$ values between −1.49 and +0.26‰ (mean value of −0.64‰). These sedimentary units host early diagenetic pyrite concretions that yield much higher Se concentrations, between 10 and 167 µg/g, with predominantly negative $\delta^{82}Se$ values between −3.0 and +0.9‰ (mean value of −1.1‰). The $\delta^{15}N$ values of both bulk samples and extracted kerogen are in the same range, between +1.3 and +4.9‰ (mean values of +3.4‰, with no systematic offset between $\delta^{15}N_{bulk}$ and $\delta^{15}N_{ker}$ values), and are much lower than $\delta^{15}N$ values recorded in the underlying FB_{1a} unit (Fig. 2, Table S2). Their TOC contents are highly variable with values between 0.6 and 17.9 wt.%, associated with $\delta^{13}C_{TOC}$ values between −33.3 and −21.7‰ (mean value of −27.8‰). The upper part of the FB_{1c} unit corresponds to a major upwelling event and Mn oxide precipitation during a deoxygenation episode (Fig. 2). Black shales of this sedimentary unit deposited in the upwelling zone have Se concentrations between 2 and 3 µg/g, but show higher, albeit near-to-zero, $\delta^{82}Se$ values (between −0.2 and 0.0‰) relative to the underlying units (Fig. 2; Table S2). Their $\delta^{15}N$ values, exclusively above +5‰ (mean value of +6.2‰, with no systematic offset between $\delta^{15}N_{bulk}$ and $\delta^{15}N_{ker}$ values), are also much higher than those for the underlying lower FB_{1c} and FB_{1b} units, but are in the same range as those for the transgressive FB_{1a} unit (Fig. 2; Table S2). The upper FB_{1c} unit has TOC contents in the 4 to 6 wt.% range and $\delta^{13}C_{TOC}$ values between −32.5 and −31.6‰ (mean value of −32.1‰), which are slightly lower than those for the lower part of the FB_1 Member.

The FB_2 Member, deposited in a predominantly oxygenated seawater column, has been inferred to represent a return to an oxygenated surface ocean following the global deoxygenation event recorded by the underlying Mn-bearing Upper FB_{1c} unit (Ossa Ossa et al., 2018). Black shales of the FB_{2a} unit have Se concentrations between 2 and 3 µg/g, with near-to-zero $\delta^{82}Se$ values at +0.2‰, whereas $\delta^{15}N$ shifts to near-zero values between −0.7 and +1.4‰ (mean value of +0.8‰, with no systematic offset between $\delta^{15}N_{bulk}$ and $\delta^{15}N_{ker}$ values), relative to the significantly higher values ($\delta^{15}N > +5$‰) recorded in the underlying Upper FB_{1c} unit deposited during a deoxygenation event (Fig. 2; Table S2). The TOC content is between 0.7 and 4.8 wt.%, with $\delta^{13}C_{TOC}$ values between −34.7 and −31.5‰ (mean value of −33.1‰). In the FB_{2b} unit, the $\delta^{82}Se$ values are negative, between −0.5 and −0.4‰ in the black shales, with Se concentrations of 1–2 µg/g (Fig. 2; Table S2). Early diagenetic pyrite concretions hosted in these FB_{2b} unit black shales yield higher Se concentrations, between 11 and 66 µg/g, with lighter $\delta^{82}Se$ values between −1.1 and −0.2‰ (mean value of −0.8‰) (Fig. 2; Table S2). The $\delta^{15}N$ values are predominantly

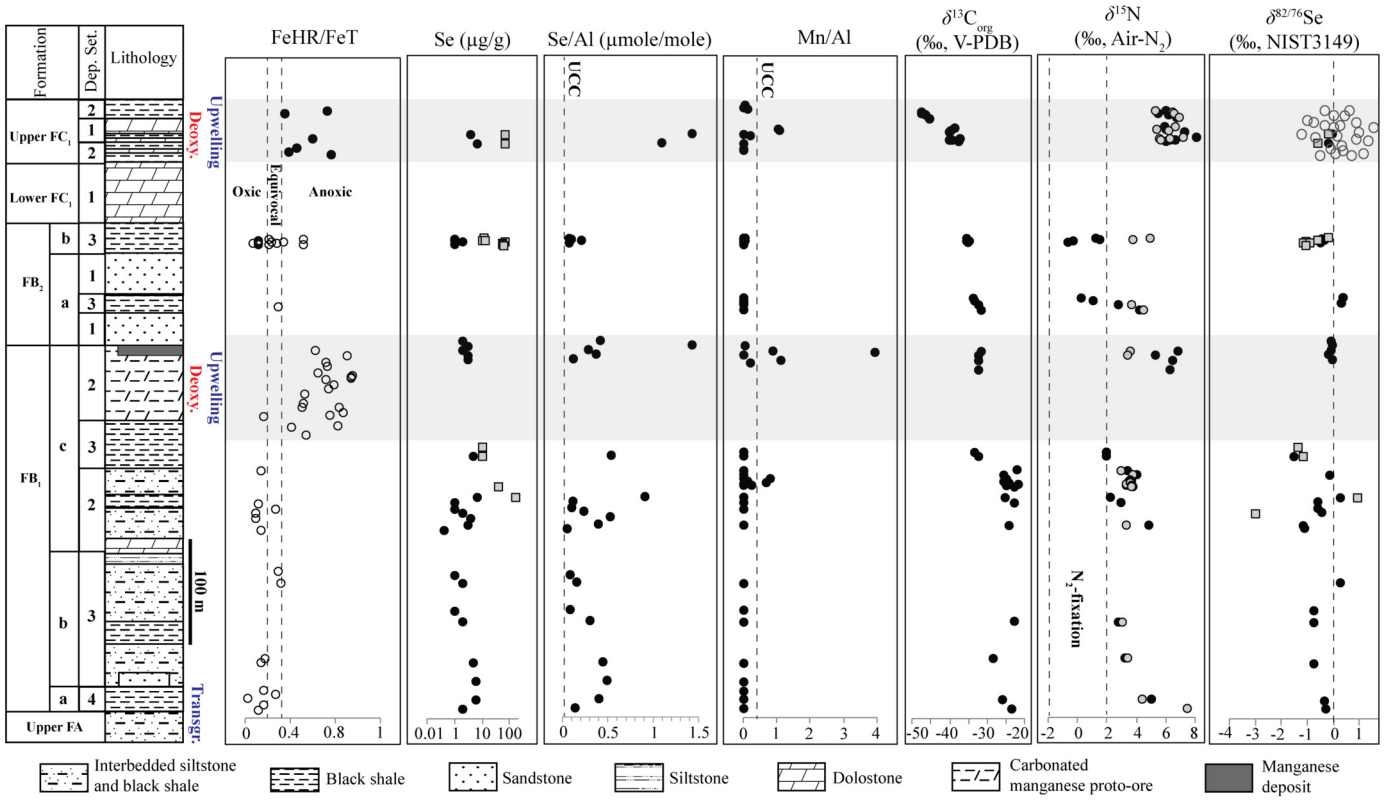

Fig. 2. Lithostratigraphic profile and geochemical data for the Francevillian Group FB and FC formations deposited during the Lomagundi Event (Ossa Ossa et al., 2013, 2018; Préat et al., 2011). Fe_{HR}/Fe_T data for the FB Formation (empty circles) are from previous work (Canfield et al., 2013; Ossa Ossa et al., 2018), while data shown as black-filled circles for the Upper FC_1 Member are from this study. Oxic, anoxic and equivocal fields are determined according to Poulton and Canfield (2011) (see Methods in Supplementary Text SI 2). Dashed lines labeled with UCC on Mn/Al and Se/Al plots represent the values for upper continental crust (Rudnick and Gao, 2014). In the Se concentration and $\delta^{82/76}Se$ plots, black-filled circles represent shale, grey-filled squares correspond to pyrite concretions, and empty, grey circles indicate previously published data from Kipp et al. (2017) and Mitchell et al. (2016). In the $\delta^{15}N$ plot, black-filled circles are for bulk samples and grey-filled circles represent extracted kerogen. In the stratigraphic log numbers refer to the depositional setting (Dep. Set.; see Supplementary text): 1 = intertidal; 2 = upper shoreface to offshore transition; 3 = lower offshore; 4 = distal outer shelf. Shaded, gray fields represent the two-step deoxygenation event recorded by the Francevillian Group (Deoxy.) and associated with upwelling of anoxic deep-waters during deposition of the upper parts of the FB_{1c} unit and FC Formation (Ossa Ossa et al., 2018). Transgr. = transgression.

close to zero and range between −1.2 and +4.8‰ (mean value of +0.4‰, with no systematic offset between $\delta^{15}N_{bulk}$ and $\delta^{15}N_{ker}$ values). The TOC and $\delta^{13}C_{TOC}$ values in the FB_{2b} unit are similar to those from the underlying FB_{2a} unit.

The last black shale unit analyzed in this study occurs in the Upper FC_1 Member, which corresponds to the end of the LE associated with a deoxygenation event (Ossa Ossa et al., 2018, 2021a). Here, Se concentrations in black shales are between 4 and 7 µg/g, and $\delta^{82}Se$ values are between −0.2 and 0.0‰ (mean value of −0.1‰), whereas early diagenetic pyrite concretions hosted in these black shales yield Se concentrations of 68–70 µg/g and $\delta^{82}Se$ values between −0.6 and −0.2‰ (mean value of −0.4‰) (Fig. 2; Table S2). $\delta^{15}N$ values shift again to exclusively positive values > +5‰ (mean value of +6.1‰, with no systematic offset between $\delta^{15}N_{bulk}$ and $\delta^{15}N_{ker}$ values) relative to the near-zero values recorded in the underlying FB_2 Member. The TOC content is between 2.0 and 18.3 wt.%, with more negative $\delta^{13}C_{TOC}$ values (−48.9 to −37.1‰, mean value of −42.8‰). Furthermore, new iron speciation data from this sedimentary unit have Fe_{HR}/Fe_T ratios > 0.38 (mean value of 0.93), while Fe_{Py}/Fe_{HR} ranges between 0.21 and 0.88 (mean value of 0.57) (Fig. 2; Table S1).

5. Discussion

As for any ancient sedimentary rock evaluated for biogeochemical signatures and redox proxies, diagenetic and secondary alteration processes need to be carefully considered. The excellent preservation of the FB shales has already been indicated (Ossa Ossa et al., 2013) and further discussion can be found in the Supplementary Information (SI 1; Fig. S3). We further infer that post-depositional alteration processes had only a minimal effect on N isotope data presented in this study (see SI 3), as demonstrated by a lack of a systematic offset between $\delta^{15}N_{bulk}$ and $\delta^{15}N_{ker}$ values (Fig. 2). Furthermore, the well-preserved pyrite concretions analyzed in this study rule out post-depositional alteration and/or surface oxidative weathering (Fig. S3). In addition, a significant effect on the Se isotope ratios of pyrite with such high Se concentrations seems unlikely, given the large amount of Se that would have had to be mobilized. Specifically for Se, the reducing conditions maintained by TOC and sulfide would have provided a strong O_2-buffer, which would not allow much (if any) soluble, oxidized Se phases to be mobilized. In view of this, the excellent preservation, combined with reducing conditions, indicate that Se and N biogeochemical signatures are well preserved and thus robust.

5.1. Redox conditions in the Francevillian water column

The average Se concentration of the Francevillian black shales (1 to 7 µg/g) shows authigenic enrichment, with high Se/Al ratios between 0.04 and 1.43 ppm/wt.%, which are considerably higher than the average UCC value of 0.01 ppm/wt.% (cf. Rudnick and Gao, 2014). While Se appears to be mainly associated with sulfide phases in the Francevillian Group black shales (see Fig. S4), this enrichment is within the range of other Paleoproterozoic and late Neoarchean sedimentary successions, and is interpreted to result from oxidative terrestrial weathering of selenium-bearing miner-

als, followed by Se sequestration into organic- and sulfide-bearing sediments (Kipp et al., 2017; Mitchell et al., 2016; Stüeken, 2017; Stüeken et al., 2015; von Strandmann et al., 2015).

The modern Se geochemical cycle is dominated by aerobic processes, with an average δ^{82}Se value of approximately +0.3‰ in seawater (Fig. S5A; Cutter and Bruland, 1984; Stüeken, 2017; Stüeken et al., 2015; von Strandmann et al., 2015). Terrestrial runoff represents the dominant Se input to the oceans (~89% of Se), with an average δ^{82}Se value within the igneous inventory range of between −0.3 to +0.3‰, while ~10% is contributed by volcanic activity and/or aerosols (Stüeken, 2017). Incorporation into organic particles (δ^{82}Se ≈ +0.3‰) and sulfide minerals (δ^{82}Se ≤ +0.3‰) in suboxic and anoxic/euxinic areas (~45 and 7% of Se, respectively), as well as adsorption onto ferromanganese oxides (δ^{82}Se ≈ +0.3‰) in oxic seawater (~48% of Se), represent the main oceanic Se output channels (Stüeken, 2017). In the modern, fully oxygenated ocean, negative sedimentary δ^{82}Se values reflect partial reduction of SeO_x^{2-} (i.e., SeO_4^{2-}, SeO_3^{2-} and $HSeO_3^-$) during diagenesis, although a similar signal may also be generated in oxygen-minimum zone (OMZ) settings overlain by oxygenated waters (Fig. 2B). Oxic water masses are enriched in dissolved Se and continuously supply Se oxyanions, which prevents quantitative Se reduction in anoxic pore-waters or in OMZ settings (Fig. S5A; Kipp et al., 2017; Mitchell et al., 2016; Stüeken, 2017; Stüeken et al., 2015; von Strandmann et al., 2015). In a strongly redox-stratified water column, sediments record positive δ^{82}Se values, similar to, or exceeding those, of local seawater, due to near-quantitative reduction where the rate of SeO_x^{2-} supply lags behind its removal (Fig. S5A; Kipp et al., 2017; Mitchell et al., 2016; Stüeken, 2017; Stüeken et al., 2015; von Strandmann et al., 2015).

In the FB Formation black shales deposited during the LE, negative δ^{82}Se values are dominant from inner to upper outer shelf depositional environments (maximum water depth around 100 m) and suggest non-quantitative reduction of SeO_x^{2-} in oxic to suboxic bottom waters and/or in sediments at the site of deposition (Fig. 2; Table S2). Predominantly negative δ^{82}Se values in the upper outer shelf are consistent with SeO_x^{2-} resupply from oxygenated lower outer shelf or much deeper water masses, as proposed for the NOE and Phanerozoic oceans (von Strandmann et al., 2015). Consequently, the seawater column in the Francevillian basin must have been fully oxygenated during the LE, including nearshore and offshore environments, with a sufficiently deep redoxcline (>100 to ~200 m deep; see SI.1) to allow for the build-up of a large SeO_x^{2-} reservoir in the surface ocean.

To distinguish between water-column and sedimentary SeO_x^{2-} reduction, we investigated selenium isotope compositions in early diagenetic pyrite concretions characterized by negative δ^{34}S (averaging −20‰) and near-to-zero Δ^{33}S values, which are considered to have formed in equilibrium with sediment pore-waters (Ossa Ossa et al., 2018). Here, pyrite has Se concentrations higher than the host sediments (having values as high as 167 µg/g), with negative δ^{82}Se values (down to −3‰) in both shallow- and deep-marine environments (Fig. 2; Table S2). The highly negative δ^{82}Se values of the FB Formation pyrite are similar to those of Jurassic, Cretaceous and modern diagenetic pyrite concretions from sediments deposited beneath an oxygenated seawater column (Table S3). Therefore, combined S-Se isotope systematics for early diagenetic FB Formation pyrite concretions show that at high partial sulfate reduction rates in the sediments, the reduction of SeO_x^{2-} (likely a selenate; SeO_4^{2-}) was not complete (König et al., 2019). Furthermore, Mn oxides, which were present as electron acceptors in Francevillian Group sediments (Canfield et al., 2013; Gauthier-Lafaye and Weber, 2003; Ossa Ossa et al., 2018, 2021b) require a redox potential higher than, or similar to, SeO_4^{2-} at circumneutral pH in marine environments (Figs. S6, S7). Therefore, SeO_4^{2-} species are also expected to have been available as electron acceptors during early diagenesis (Canfield et al., 2013; Gauthier-Lafaye and Weber, 2003; Ossa Ossa et al., 2018, 2021b). Incomplete diagenetic SeO_x^{2-} reduction thus further supports a continuous supply of SeO_4^{2-}, a fully oxygenated water column in the open-marine Francevillian basin, and a redoxcline likely situated much deeper in the water column, below the outer shelf, during the LE (Figs. 2; SI.1).

Nevertheless, three intervals spanning inner- and outer-shelf environments record small positive δ^{82}Se values in black shales, with one of these intervals having a diagenetic pyrite concretion with higher positive δ^{82}Se values (Fig. 2; Table S2). These positive values may have resulted from near-quantitative Se reduction under anoxic seawater conditions, but this interpretation is incompatible with highly negative δ^{34}S values, low Fe_{HR}/Fe_T, V/Al, Mo/Al and U/Al ratios for the black shales, which suggest oxic bottom waters at the site of deposition during a period of high marine sulfate concentration (Fig. 2; Canfield et al., 2013; Ossa Ossa et al., 2018, 2021a, 2021b). We thus interpret the positive δ^{82}Se value of +0.9‰ for this early diagenetic pyrite concretion to reflect complete Se reduction in the sediments, as proposed for the Cretaceous Navajún pyrite (König et al., 2019), while the host shale δ^{82}Se values of +0.2 to +0.3‰ represent biomass accumulation, potentially recording seawater Se isotope composition (Stüeken, 2017; von Strandmann et al., 2015). Such conditions may have been due to a higher rate of organic carbon sequestration causing extensive anoxia during early diagenesis, thus likely exhausting the availability of electron acceptors, and/or Se assimilation into biomass, perhaps due to an overall lower seawater SeO_4^{2-} reservoir during deposition. In the latter case, SeO_4^{2-} might have been more sensitive to mild redox changes under moderately suboxic conditions in the Francevillian basin seawaters than redox proxies based on Fe and S.

For the upper part of the FC Formation black shales, the δ^{82}Se data show near-to-zero to slightly negative values, which may be interpreted in different ways (Stüeken, 2017). However, our new Fe speciation data indicate deposition under euxinic to anoxic, ferruginous conditions (Figs. 2, S2B; Table S1). Furthermore, previously published δ^{82}Se data from a much higher resolution sample set from this sedimentary succession show predominantly positive to near-to-zero values and minor negative values (Fig. 2; Kipp et al., 2017; Mitchell et al., 2016), which is consistent with an euxinic to anoxic/suboxic setting. Indeed, a strongly redox-stratified marine setting, with a shallow redoxcline, has been proposed for the upper part of the FC Formation (Kipp et al., 2017; Ossa Ossa et al., 2018, 2021a). Collectively, trace elements (V, U, Mo), Fe speciation and δ^{82}Se data for the upper part of the FC Formation support deposition under anoxic seawater conditions, following upwelling of Fe^{2+}- and Mn^{2+}-rich anoxic waters during a period of enhanced submarine volcanic activity at the end of the LE (Fig. 2; Ossa Ossa et al., 2018, 2021a).

5.2. Biogeochemical nitrogen cycle during the LE

Modern oceans are characterized by an aerobic N cycle, where nitrate (NO_3^-) is the major dissolved species and carries a positive δ^{15}N signature (averaging ~ +5‰ with respect to present-day atmospheric N_2, which, by definition, has a δ^{15}N value of 0‰; Ader et al., 2016; Sigman and Fripiat, 2019). This isotopic enrichment is mainly controlled by partial loss of nitrate through water-column denitrification and/or anammox in OMZs (Ader et al., 2016; Sigman and Fripiat, 2019; Stüeken et al., 2016). Nitrate-assimilating biomass indirectly preserves the isotopic composition of dissolved nitrate in marine sediments (Fig. S5B). By contrast, under anoxic conditions, where nitrate is typically absent from the water column, the N isotope composition of biomass is controlled by bio-

logical N_2 fixation, with $\delta^{15}N$ values in the range of -3 to $+1$‰ (Ader et al., 2016; Sigman and Fripiat, 2019; Stüeken et al., 2016), with only rare examples down to ~ -7‰ (Zhang et al., 2014). Interpretations of N isotope data from ancient sedimentary rocks have been challenged on the basis that the N isotopic composition of the atmosphere may have changed over time (e.g., Jia and Kerrich, 2004; Kerrich et al., 2006). However, N isotope analyses of fluid inclusions in cherts have shown that the $\delta^{15}N$ value of atmospheric N_2 has likely stayed close to 0‰ since at least ca. 3.5 Ga (Sano and Pillinger, 1990; Marty et al., 2013). Therefore, $\delta^{15}N$ values $> +2$‰ in ancient unaltered marine sedimentary rocks are generally interpreted to reflect the operation of an aerobic N cycle (e.g., Fig. S5B; Ader et al., 2016; Cheng et al., 2019; Kipp et al., 2018; Stüeken et al., 2016; Zerkle et al., 2017).

The Francevillian Group black shales are dominated by $\delta^{15}N$ values in the range of -2 to $+3$‰ (average $+1 \pm 3$‰), with positive shifts of > 5‰ (having no relationship to water depth) at three stratigraphic levels (Fig. 2; Table S2). The assumed low degree of post-depositional alteration of the N isotope data suggests that the $\delta^{15}N$ values obtained for the studied FB and FC formations OM-rich shale and silty shale samples should provide a best estimate of the primary isotopic composition of middle Paleoproterozoic sediments and organic matter (see SI 3; Figs. 2, S8). Combined Fe speciation, $\delta^{82}Se$, $\delta^{34}S$ and trace metal concentration data indicate deposition under a well-oxygenated water column. By contrast, a few samples with elevated Fe_{HR}/Fe_T (> 0.38) ratios from the FB_{2b} unit, as well as the predominantly small $\delta^{15}N$ values of $+1 \pm 3$‰ in the FB Formation (Fig. 2; Table S2), could be interpreted to reflect deposition under anoxic water-column conditions with a purely anaerobic N cycle. However, these elevated Fe_{HR}/Fe_T ratios and low $\delta^{15}N$ values contrast with negative $\delta^{82}Se$ values, low V/Al, low Mo/Al, and low U/Al ratios that are suggestive of oxic water column conditions (Ossa Ossa et al., 2021a; Fig. 2). We propose that the elevated Fe_{HR}/Fe_T ratios more likely represent upwelling of deep anoxic waters onto oxic shallow shelves (potentially changing the chemocline depth), causing precipitation of iron from the water column. Hence, considering this generally oxic setting, it is unlikely that these low $\delta^{15}N$ values reflect a purely anaerobic N cycle. Instead, we interpret the N isotope data to reflect quantitative nitrification in an oxic seawater column, while denitrification mainly occurred in sediments, which typically results in very small isotopic effects ($\delta^{15}N$ values of $+1 \pm 3$‰).

This interpretation further suggests that the redoxcline (at which water-column denitrification occurs and imparts large fractionations in $\delta^{15}N$) was generally situated much deeper on the outer shelf (maximum water depth < 200 m; SI 1), or even below it, and that the Francevillian basin was not connected to a larger, isotopically fractionated marine NO_3^- reservoir during deposition of the FB and FC formations. One possible explanation might be that the basin was restricted at this time. However, this seems unlikely because the FB and FC formations record the LE, which was a typical feature of the open ocean (Bekker, 2022; Bekker et al., 2003; Karhu and Holland, 1996). Furthermore, trace metal enrichments (V, Mo and U) in the upper part of the FC Formation (Ossa Ossa et al., 2021a) indicate that the Francevillian basin was likely connected to the global ocean. Rather, we suggest that the open ocean did not contain a significant NO_3^- pool that could have mixed with, and isotopically influenced, the nitrogen cycle in shallow-water settings. If the offshore marine NO_3^- pool was indeed small, biological N_2 fixation rather than NO_3^- assimilation would have been the major N uptake process, similar to some Mesoarchean and Mesoproterozoic marine settings or the modern Black Sea, and this may have contributed to dissolved N (likely ammonium) with low $\delta^{15}N$ values in the biological N_2 fixation range (Ader et al., 2016; Ossa Ossa et al., 2019; Stüeken et al., 2016). Mixing of this negligible ammonium reservoir (with low $\delta^{15}N$ values) with the shallow-marine, isotopically unfractionated nitrate reservoir would explain the relatively low $\delta^{15}N$ values observed in the shallow-marine sediments.

Positive $\delta^{15}N$ values, between $+5$ and $+8$‰, recorded during the three episodes of redoxcline encroachment into shallow-marine environments indicate that, during these intervals, NO_3^- concentrations were high enough to allow only partial water-column denitrification. The residual isotopically enriched NO_3^- pool was evidently large enough to be assimilated into biomass followed by subsequent preservation in the sediments (Figs. 2, 3). This is further supported by previously published N isotope data for the upper part of the FC Formation ($\delta^{15}N > +5$‰), indicating partial water-column denitrification and/or anammox, with a NO_3^- pool that was large enough to leave an isotopic signature of strong redox cycling of nitrogen in the water column (Kipp et al., 2018).

Importantly, deposition of the upper parts of the FB_{1c} unit and FC Formation coincided with a global two-step deoxygenation event during a period of enhanced submarine volcanic activity at the end of the LE (Ossa Ossa et al., 2018). Associated with these phenomena, an episodic redoxcline encroachment onto the inner shelf would have locally provided anoxic conditions for partial denitrification and/or anammox in the water-column, which is supported by highly negative $\delta^{13}C_{TOC}$ values (down to -48‰, V-PDB), reflecting enhanced activity of heterotrophs (e.g., methanotrophs and denitrifiers) in the water column during these two deoxygenation events (Figs. 2, 3; Table S2; Ossa Ossa et al., 2018). Before these events, the NO_3^- reservoir progressively grew as a result of enhanced oxygenic photosynthesis during the LE, which resulted in an expansion of oxygenated conditions in the Francevillian basin from the shelf edge to outer shelf. This scenario implies availability of free O_2, at least at the level of a few µM, to allow buildup of NO_3^- above the redoxcline. Nitrate reduction becomes pervasive when dissolved oxygen is below ~2 µM (Lam and Kuypers, 2011), which is equivalent to roughly 1% of modern seawater dissolved oxygen in equilibrium with the atmosphere. Hence, seawater dissolved oxygen at the depositional site of the upper parts of the FB_{1C} unit and FC Formation appears to have been above this threshold. Our combined N and Se isotope data thus provide a minimum level of 1% modern marine O_2 saturation level for the dissolved oxygen content of seawater at the end of the LE.

Another sedimentary succession, the lower ca. 2.1–2.0 Ga Zaonega Formation of Russia (see Ossa Ossa et al., 2018, 2021a for detailed discussion on the depositional age), where Fe speciation and trace-metal data suggest deposition under oxic conditions during the late stage of the LE (Canfield et al., 2013; Scott et al., 2014), also shows a correlation between extracted kerogen $\delta^{15}N$ values $< +2$‰ (Kump et al., 2011) and light $\delta^{82}Se$ values (Fig. 4; Table S3). By contrast, the upper part of the Zaonega Formation, which was deposited during the deoxygenation event at the end of the LE (Asael et al., 2018; Canfield et al., 2013; Kump et al., 2011; Scott et al., 2014), yielded more positive $\delta^{15}N$ values of $> +2$‰ for extracted kerogen (Kump et al., 2011) and more positive $\delta^{82}Se$ values (Fig. 4; Table S3). Combined, the Francevillian Group and the lower Zaonega Formation N and Se isotope data show parallel trends associated with similar seawater redox changes. Continental-shelf black shales with near-to-zero $\delta^{15}N$ values of extracted kerogen are also known from several other sedimentary successions recording the LE, including the ca. 2.2 Ga Wewe Slate, ca. 2.15 Ga Sengoma Argillite Formation, and ca. 2.1 Ga Hautes Chute Formation (Kipp et al., 2018). Collectively, this indicates that oxic conditions with small seawater NO_3^-- and SeO_4^{2-}-reservoirs, episodically affected by an encroaching redoxcline, were a common feature in marginal-marine basins across the LE until its end. Hence, enhanced biological O_2 production drove pervasive oxygenation in

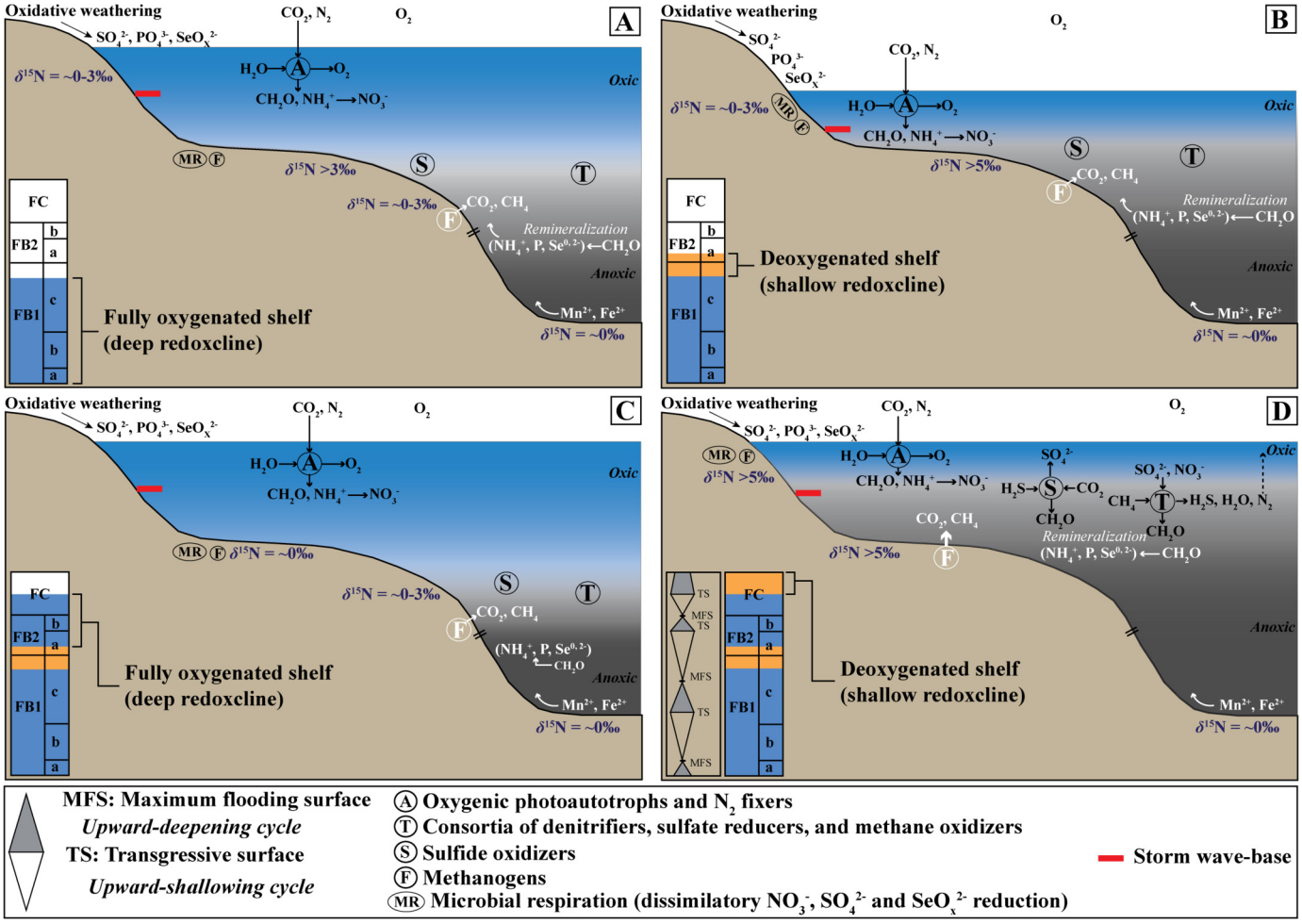

Fig. 3. Reconstruction of paleoenvironmental changes during deposition of the Francevillian Group showing a fully oxygenated, continental-shelf water column having a minor expression of N aerobic cycle with predominantly sedimentary denitrification and relatively deep redoxcline in the ocean during the LE (e.g., **A** and **C**). Episodes of redoxcline encroachment into shallow-marine environments led to the development of extensive anoxic conditions on the continental shelf that enhanced local consumption of NO_3^{--} in the water column and caused a stronger local isotopic expression of aerobic N cycle at the end of the LE (e.g., **B** and **D**). Full metabolic reactions for T (consortia of denitrifiers, sulfate reducers and methane oxidizers) and S (sulfide oxidizers) as well as variations in sea level are only shown in **D** for clarity.

shelf environments, which likely shifted the redoxcline deeper in the water column to allow growth of the O_2, NO_3^- and SeO_4^{2-} pools in open, marginal-marine settings during the LE (Fig. 3).

5.3. Implications for Earth surface oxygenation during the LE

Based on the molybdenum isotope records of black shales deposited during the GOE, it has been inferred that the oceans were redox-stratified and largely anoxic, but with pulsed intervals of progressively expanding euxinia from the early stage of the GOE (ca. 2.43 Ga) to its termination (ca. 2.06 Ga) (Asael et al., 2018). This view is also supported by previously published Se isotope data for contemporaneous continental-shelf black shales, which are dominated by positive δ^{82}Se values (Fig. 5; Kipp et al., 2017; Mitchell et al., 2016; Stüeken et al., 2015), inferred to reflect quantitative SeO_x^{2-} reduction in strongly redox-stratified oceans with a shallow redoxcline situated above storm wave-base (Fig. 5; Kipp et al., 2017). The predominantly positive δ^{15}N values ($> +4‰$) in these black shales deposited during the early stage of the GOE—before the LE— are also consistent with partial water-column denitrification and anammox in strongly redox-stratified oceans with a significant nitrate reservoir in the oxic surface layer (Cheng et al., 2019; Kipp et al., 2018; Stüeken et al., 2016), similar to that inferred for the two-step deoxygenation event at the end of the LE recorded in the Francevillian basin (Figs. 2, 3; Table S2). It thus appears that positive δ^{15}N values recorded in marginal-marine settings at the beginning and end of the GOE—before and immediately after the LE—reflect a locally enhanced isotopic expression of partial water-column denitrification and/or anammox, as a consequence of redox stratification. A minimum O_2 surface ocean concentration of >0.4 μM has been proposed during these two time intervals, based on Se isotope data alone (Kipp et al., 2017). Our combined N and Se isotope data increase the minimal seawater dissolved O_2 concentration to >2 µM for the later timer interval.

Molybdenum isotope data show that during the LE, the ocean redox state evolved towards the more expansive development of oxic conditions, before returning at the end of the LE to oceans with a shallow redoxcline and extensive development of euxinic conditions (Asael et al., 2018). High I/(Ca+Mg) ratios in shallow-water carbonates, which are interpreted to reflect a substantial IO_3^- reservoir in the surface ocean, with dissolved O_2 concentrations of at least 1 µM, agree with more expansive seawater oxygenation during the LE (Hardisty et al., 2014), although offshore environments—outer shelf and beyond—are inferred to have remained anoxic (Kipp et al., 2017; Stüeken et al., 2016). Our data show a small range in δ^{15}N values ($+1 \pm 3‰$), combined with predominantly negative δ^{82}Se values, for sediments deposited below storm wave-base, suggesting extensive oxygenation of the lower outer shelf during the LE (Figs. 2, 3). Dissolved NO_3^- with a maximum concentration of ~4 µM (Cheng et al., 2019) has been sug-

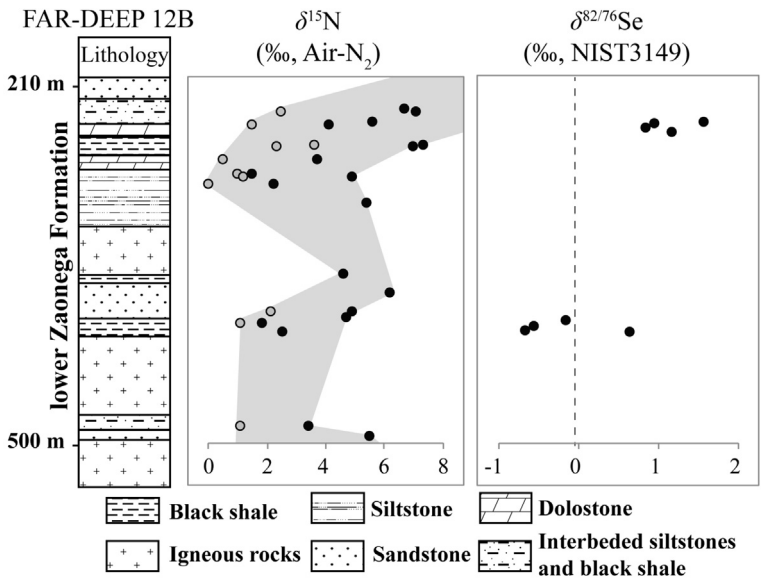

Fig. 4. Co-variation among $\delta^{15}N_{bulk}$, $\delta^{15}N_{ker}$ (kerogen fraction) and $\delta^{82/76}Se$ data for the lower Zaonega Formation, Russia (FAR-DEEP drill-core 12B). Nitrogen isotope data are from Kump et al. (2011). The highest $\delta^{15}N_{bulk}$ values in the lowermost part are from sandstone and may be due to post-depositional alteration (as indicated by a marked offset between $\delta^{15}N_{bulk}$ and $\delta^{15}N_{ker}$ values), while $\delta^{15}N_{bulk}$ and $\delta^{15}N_{ker}$ values in shales are closer to each other and may reflect primary N isotopic composition, which corresponds to lighter Se isotopic composition in the lower section. Both $\delta^{15}N_{bulk}$ and $\delta^{15}N_{ker}$ values increase in the upper part of the lower Zaonega Formation and correspond to higher Se isotope values. On the $\delta^{15}N$ plots, black-filled circles are for bulk samples and grey-filled circles represent extracted kerogen.

gested for proximal-shelf marine environments during the early stage of the GOE (Cheng et al., 2019; Kipp et al., 2018; Stüeken et al., 2016), and such conditions might have developed, at least episodically, as early as the Neoarchean (cf. Stüeken et al., 2016 and references therein). However, this NO_3^- pool did not reach a pervasive and stable level in offshore environments situated on the lower part of the outer shelf during the Paleoproterozoic (Cheng et al., 2019; Kipp et al., 2018; Stüeken et al., 2016). Our combined N and Se isotope data show for the first time that the NO_3^- and SeO_4^{2-} reservoirs were persistent and stable across the entire continental shelf during the LE (Fig. 3). This requires a much higher rate of oxidant accumulation, with O_2 and NO_3^- concentrations well above the minimum levels reached during the early stage and end of the GOE, which indicates enhanced biological O_2 production in the surface ocean. Such a high rate of oxygenic photosynthesis in shallow-marine environments must have caused O_2 downwelling, resulting in a deeper position of the redoxcline in the water column (Fig. 5), which nevertheless likely remained shallower than in the NOE oceans (Alcott et al., 2019; Canfield et al., 2007; Lenton et al., 2014; von Strandmann et al., 2015).

Thick sulfate evaporite deposits, consistent with high seawater sulfate concentrations and developed in a supposedly marginal-marine basin during the LE, have been linked to the buildup of an oxidant reservoir equivalent to more than 20% of the modern atmosphere-ocean oxidizing capacity (Blättler et al., 2018). However, an open-marine setting for this succession in the Onega basin on the Karelia craton has been recently questioned on sedimentological and geochemical grounds (Alfimova et al., 2022), and an apparently large thickness of the sulfate evaporite deposit might reflect a drill core intersection through the central part of a salt diapir rather than true stratigraphic thickness (cf. Esipko et al., 2014). Furthermore, based on large U and Cr isotope fractionations recorded in black shales deposited at the end of the LE, it has been proposed that the middle Paleoproterozoic oceans remained well-oxygenated even after the end of the LE, and that modern-style biogeochemical cycling developed during the middle Paleoproterozoic (Mänd et al., 2020, 2022). However, the Cr and U isotope data can be explained by slow depositional rates and the removal of redox-sensitive elements from the oceans under suboxic to weakly euxinic settings after the GOE. Furthermore, large Cr and U isotope fractionations, which have not been systematically recognized in sedimentary deposits until the Neoproterozoic (e.g., Dang et al., 2022; Planavsky et al., 2014), may alternatively suggest that these redox-sensitive elements were drawn from a relatively small seawater reservoir, either in the whole ocean or in somewhat isolated basins (see Andersen et al., 2020; Dang et al., 2022). Considering the regional stratigraphic framework for Karelia in Finland and Russia, where multiple sedimentary basins record flooding at the end of the Lomagundi carbon isotope excursion, as also recorded by the Zaonega Formation, it appears that these large U and Cr isotope variations over short stratigraphic intervals likely reflect a very small U and Cr reservoir in the ocean. It is also important to emphasize that multistage reduction-oxidation processes subsequent to deposition and in association with hydrothermal fluid or hydrocarbon migration, as well as a wide range of redox-independent processes, could fractionate Cr and U isotopes regardless of ocean dissolved oxygen content (Andersen et al., 2020; Babechuk et al., 2017, 2018; Dang et al., 2022; Miletto et al., 2021), which limits their application to infer O_2 levels in the atmosphere-ocean system.

Regardless of this difference in interpretation, in contrast to N and Se, S and U yield oxyanions that are stable at low Eh (< 0 V; Figs. S6, S7; Rue et al., 1997; Stumm and Morgan, 1970) under the circumneutral pH conditions of the Paleoproterozoic oceans (Halevy and Bachan, 2017). Although our combined N and Se isotope data support extensive ocean oxygenation during the LE, it appears that the NO_3^- inventory was not sufficient to shift the N isotopic composition of the global ocean. A model arguing for biogeochemical cycling comparable with the oxidant reservoir approaching the size of the modern atmosphere-ocean capacity (Blättler et al., 2018; Mänd et al., 2020) thus seems unlikely for the middle Paleoproterozoic. Moreover, the N and Se isotope data indicate that the oxyanions of these two elements, which are redox-sensitive at a higher redox potential (Eh > 0.4 V at circumneutral pH; Figs. S6, S7, S1), were more attuned to O_2 dynamics in the atmosphere-ocean system across the GOE, compared to S- and U-based proxies. Indeed, N and Se isotope data record progressive oxygenation of the atmosphere-ocean system from the beginning

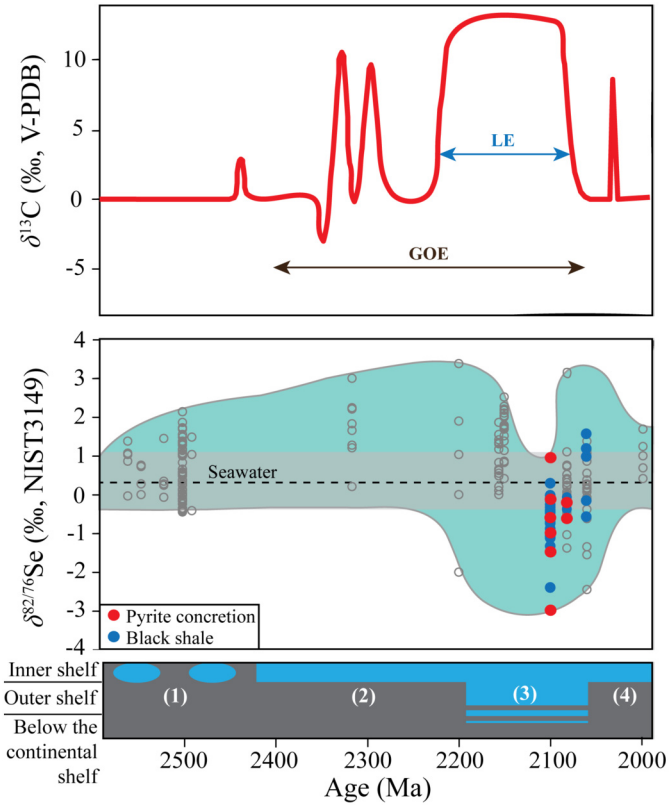

Fig. 5. Evolution of ocean redox seascape during the GOE, indicating progressive oxygenation of the oceans. Predominantly negative $\delta^{82/76}$Se values during the peak of the LE mark the development of a relatively deep redoxcline in the water column. The upper panel shows δ^{13}C values for marine carbonates compiled from the literature (Bekker, 2022; Bekker et al., 2003, 2016; Bekker and Holland, 2012; Karhu and Holland, 1996; Ossa Ossa et al., 2018; Planavsky et al., 2012). The lower panel shows the distribution of oxic (blue) vs. anoxic (grey) conditions in the water column. (**1**) = predominantly anoxic ocean with oxygen oases in sublittoral zone (e.g., Lyons et al., 2014; Kipp et al., 2017; Stüeken et al., 2016); (**2, 4**) = redox-stratified oceans with the maximum depth of the redoxcline above the storm wave-base; (**3**) = redox-stratified ocean with a relatively deep redoxcline in the distal outer shelf or below. Empty circles are $\delta^{82/76}$Se data from previous studies (Kipp et al., 2017; Mitchell et al., 2016; Stüeken, 2017; Stüeken et al., 2015) ($\delta^{82/76}$Se = 1.5*$\delta^{82/78}$Se). Filled circles represent $\delta^{82/76}$Se data from this study. Shaded, grey field represents $\delta^{82/76}$Se range of modern seawater. (For interpretation of the colors in the figure(s), the reader is referred to the web version of this article.)

of the GOE to the LE, which is not clearly expressed in S and U isotope data (e.g., Blättler et al., 2018; Holland, 2006; Mänd et al., 2020; Ossa Ossa et al., 2018; Planavsky et al., 2012; Scott et al., 2014). Furthermore, N and Se isotope data also record widespread ocean deoxygenation at the end of the LE/GOE that is not obvious in U and Mo isotope records (Mänd et al., 2020; but see Asael et al., 2018 and Andersen et al., 2020 for a different view on secular Mo and U isotope variations). Development of deoxygenated marine conditions at the end of the LE is further supported by high V enrichment in black shales (Asael et al., 2018; Ossa Ossa et al., 2018; Scott et al., 2014), which reflects strong anoxia in open, continental-shelf settings (Canfield et al., 2013; Ossa Ossa et al., 2021a). Anoxic seawater conditions at the end of the LE does not imply that these oceanic conditions remained steady until the NOE, and indeed, several local to potentially global mid-Proterozoic oxygenation events have recently been described (Canfield et al., 2018; Dang et al., 2022; Luo et al., 2021; Stüeken et al., 2021; Zhang et al., 2018). The evolving picture of oxygen dynamics in the Paleoproterozoic atmosphere-ocean system thus highlights an increase in the amplitude of oxygenation from the beginning of the GOE to the LE, with superimposed smaller scale oxygen oscillations. This implies that, despite transiently elevated oxygen concentrations during the LE, feedbacks linking terrestrial weathering, nutrient controls on primary organic productivity, and low oxygen levels maintained the atmosphere-ocean system at an oxygenation state far below the modern level.

6. Conclusions

Dissolved nitrate was heterogeneous and unstable in offshore marine environments during the ca. 2.43–2.06 Ga GOE. By contrast, new combined Se and N isotope data presented here show that continental shelf waters were highly oxygenated, with unlimited supply of nitrate and selenium oxyanions during the peak of the LE. Although enhanced accumulation of oxidants clearly demonstrates high rates of oxygenic photosynthesis in shallow-marine environments during the LE, the oceanic O_2 inventory remained well below the modern level. Pervasive redox stratification in the deep oceans during the LE implies that the global extent of modern biogeochemical cycles and their isotopic effects were not achieved until the end of the Neoproterozoic.

CRediT authorship contribution statement

Conception and design of the study: Frantz Ossa Ossa and Ronny Schoenberg; **Field sampling:** Frantz Ossa Ossa, Axel Hofmann, Andrey Bekker and Ronny Schoenberg; **Acquisition of data:** Frantz Ossa Ossa, Jorge E. Spangenberg, Stephan König, Eva E. Stüeken, Simon W. Poulton, Aierken Yierpan and Maria Isabel Varas-Reus; **Interpretation of data:** Frantz Ossa Ossa with significant contribution from Ronny Schoenberg, Eva E. Stüeken, Andrey Bekker and Simon W. Poulton; **Drafting the article:** Frantz Ossa Ossa; **Revising the article critically for important intellectual content:** Frantz Ossa Ossa, Jorge E. Spangenberg, Andrey Bekker, Stephan König, Eva E. Stüeken, Axel Hofmann, Simon W. Poulton, Aierken Yierpan, Maria Isabel Varas-Reus, Morten B. Andersen, Benjamin Eickmann and Ronny Schoenberg; **Final approval of the version to be submitted:** Frantz Ossa Ossa, Jorge E. Spangenberg, Andrey Bekker, Stephan König, Eva E. Stüeken, Axel Hofmann, Simon W. Poulton, Aierken Yierpan, Maria Isabel Varas-Reus, Morten B. Andersen, Benjamin Eickmann and Ronny Schoenberg.

Declaration of competing interest

The authors declare that they have no known competing financial interests or personal relationships that could have appeared to influence the work reported in this paper.

Acknowledgements

FOO and RS acknowledge financial support from the University of Tübingen and the German Research Foundation (DFG Grant SCHO1071/11-1). FOO and MBA are thankful for support from the Natural Environment Research Council (NERC grant NE/V004824/1). The stable isotope facilities at IDYST were funded by the University of Lausanne. SK, YA and MIV-R acknowledge European Research Council (ERC) Starting Grant 636808 (O2RIGIN). AH and FOO acknowledge support from National Research Foundation of South Africa (NRF Grant 75892). SK also acknowledges the Ramon y Cajal contract (RYC2020-030014-I). Participation by AB was supported by Discovery and Accelerator Grants from the Natural Sciences and Engineering Research Council of Canada (NSERC) and ACS PF grant (624840ND2). EES acknowledges funding from a NERC Frontiers grant (NE/V010824/1). SWP acknowledges support from a Royal Society Wolfson Research Merit Award. MIV-R additionally acknowledges funding support from the German Research Foundation (DFG Grant VA 1568/1-1). Bruce Cairncross is thanked for providing modern pyrite concretions from Richards Bay, South

Africa. We acknowledge the helpful comments by Kaarel Mänd, an anonymous reviewer and the handling editor, Boswell Wing, which greatly helped to increase the quality of the manuscript. We also thank Johnathan Mboulou Ella for his tremendous logistic support in the field.

Appendix A. Supplementary material

Supplementary material related to this article can be found online at https://doi.org/10.1016/j.epsl.2022.117716.

References

Ader, M., et al., 2016. Interpretation of the nitrogen isotopic composition of Precambrian sedimentary rocks: assumptions and perspectives. Chem. Geol. 429, 93–110.

Alcott, L.J., Mills, B.J.W., Poulton, S.W., 2019. Stepwise Earth oxygenation is an inherent property of global biogeochemical cycling. Science 366, 1333–1337.

Alcott, L.J., et al., 2020. Development of Iron Speciation Reference Materials for Palaeoredox Analysis. Geostand. Geoanal. Res. 44, 581–591.

Alfimova, N.A., Kuznetsov, A.B., Klimova, E.V., Bekker, A., 2022. Archean-Proterozoic unconformity on the Fennoscandian Shield: geochemistry and Sr, C and O isotope composition of Paleoproterozoic carbonate-rich regolith from Segozero Lake (Russian Karelia). Precambrian Res. 368, 106459.

Andersen, M.B., Matthews, A., Bar-Matthews, M., Vance, D., 2020. Rapid onset of ocean anoxia shown by high U and low Mo isotope compositions of sapropel S1. Geochem. Perspect. Lett. 15, 10–14.

Asael, D., Rouxel, O., Poulton, S.W., Lyons, T.W., Bekker, A., 2018. Molybdenum record from black shales indicates oscillating atmospheric oxygen levels in the early Paleoproterozoic. Am. J. Sci. 318, 275–299.

Babechuk, M.G., Kleinhanns, I.C., Schoenberg, R., 2017. Chromium geochemistry of the ca. 1.85 Ga Flin Flon paleosol. Geobiology 15, 30–50.

Babechuk, M.G., Kleinhanns, I.C., Reitter, E., Schoenberg, R., 2018. Kinetic stable Cr isotopic fractionation between aqueous Cr(III)-Cl-H_2O complexes at 25 °C: implications for Cr(III) mobility and isotopic variations in modern and ancient natural systems. Geochim. Cosmochim. Acta 222, 383–405.

Bekker, A., 2022. Huronian Glaciation. In: Gargaud, M. (Ed.), Encyclopedia of Astrobiology. Springer-Verlag.

Bekker, A., Holland, H.D., 2012. Oxygen overshoot and recovery during the early Paleoproterozoic. Earth Planet. Sci. Lett. 317–318, 295–304.

Bekker, A., Karhu, J.A., Eriksson, K.A., Kaufman, A.J., 2003. Chemostratigraphy of Paleoproterozoic carbonate successions of the Wyoming Craton: tectonic forcing of biogeochemical change? Precambrian Res. 120, 279–325.

Bekker, A., Holland, H.D., Wang, P.-L., Rumble, D., Stein, H.J., Hannah, J.L., Coetzee, L.L., Beukes, N.J., 2004. Dating the rise of the atmospheric oxygen. Nature 427, 117–120.

Bekker, A., Krapež, B., Müller, S.G., Karhu, J.A., 2016. A short-term, post-Lomagundi positive C isotope excursion at c. 2.03 Ga recorded by the Wooly Dolomite, Western Australia. J. Geol. Soc. Lond. 173, 689–700.

Blättler, C.L., et al., 2018. Two-billion-year-old evaporites capture Earth's great oxidation. Science 360, 320–323.

Bros, R., Stille, P., Gauthier-Lafaye, F., Weber, F., Clauer, N., 1992. Sm-Nd isotopic dating of Proterozoic clay material: an example from the Francevillian sedimentary series, Gabon. Earth Planet. Sci. Lett. 113, 207–218.

Canfield, D.E., Poulton, S.W., Narbonne, G.M., 2007. Late-Neoproterozoic deep-ocean oxygenation and the rise of animal life. Science 315, 92–95.

Canfield, D.E., et al., 2013. Oxygen dynamics in the aftermath of the Great Oxidation of Earth's atmosphere. Proc. Natl. Acad. Sci. USA 110, 16736–16741.

Canfield, D.E., et al., 2018. A Mesoproterozoic iron formation. Proc. Natl. Acad. Sci. USA 115, E3895–E3904.

Catling, D.C., Zahnle, K.J., 2020. The Archean atmosphere. Sci. Adv. 6, eaax1420.

Cheng, C., et al., 2019. Nitrogen isotope evidence for stepwise oxygenation of the ocean during the Great Oxidation Event. Geochim. Cosmochim. Acta 261, 224–247.

Colwyn, D.A., et al., 2019. A paleosol record of the evolution of Cr redox cycling and evidence for an increase in atmospheric oxygen during the Neoproterozoic. Gebiology. https://doi.org/10.1111/gbi.12360.

Cutter, G.A., Bruland, K.W., 1984. The marine biogeochemistry of selenium: a re-evaluation. Limnol. Oceanogr. 29, 1179–1192.

Dang, D.H., Wang, W., Gibson, T.M., Kunzmann, M., Andersen, M.B., Halverson, G.P., Evans, R.D., 2022. Authigenic uranium isotopes of late Proterozoic black shale. Chem. Geol. 588, 120644.

Dennen, K.O., et al., 2006. delta ^{15}N and non-carbonate delta ^{13}C values for two petroleum source rock reference materials and a marine sediment reference material. USGS, 2006–1071.

Esipko, O.A., Neronova, I.V., Sharov, N.V., 2014. Geophysical Study of the Onega Parametric Borehole, Lennex Corp. Nobel Press, Moscow, Russia, p. 62.

Farquhar, J., Bao, H., Thiemens, M., 2000. Atmospheric Influence of Earth's Earliest Sulfur Cycle. Science 289, 756.

Gauthier-Lafaye, F., Weber, F., 2003. Natural nuclear fission reactors: time constraints for occurrence, and their relation to uranium and manganese deposits and to the evolution of the atmosphere. Precambrian Res. 120, 81–100.

Halevy, I., Bachan, A., 2017. The geologic history of seawater pH. Science 355, 1069–1071.

Hannah, J.L., Stein, H.J., Bekker, A., Markey, R.J., Holland, H.D., 2003. Chondritic initial $^{187}Os/^{188}Os$ in Paleoproterozoic shale (seawater) and the onset of oxidative weathering. Geochim. Cosmochim. Acta 67, A-34.

Hardisty, D.S., et al., 2014. An iodine record of Paleoproterozoic surface ocean oxygenation. Geology 42, 619–622.

Holland, H.D., 2006. Oxygenation of the atmosphere and oceans. Philos. Trans. R. Soc. B 361, 903–915.

Horie, K., Hidaka, H., Gauthier-Lafaye, F., 2005. U-Pb geochronology and geochemistry of zircon from the Franceville series at Bidoudouma, Gabon. Geochim. Cosmochim. Acta 69, A11.

Husson, J.M., Peters, S.E., 2017. Atmospheric oxygenation driven by unsteady growth of the continental sedimentary reservoir. Earth Planet. Sci. Lett. 460, 68–75.

Jia, Y., Kerrich, R., 2004. A reinterpretation of the crustal N-isotope record: evidence for a ^{15}N-enriched Archean atmosphere? Terra Nova 16, 102–108.

Kanzaki, Y., Murakami, T., 2016. Estimates of atmospheric O_2 in the Paleoproterozoic from paleosols. Geochim. Cosmochim. Acta 174, 263–290.

Karhu, J.A., Holland, H.D., 1996. Carbon isotopes and the rise of atmospheric oxygen. Geology 24, 867–870.

Kerrich, R., Jia, Y., Manikyamba, C., Naqvi, S.M., 2006. Secular variations of N-isotopes in terrestrial reservoirs and ore deposits. In: Kesler, S.E., Ohmoto, H. (Eds.), Evolution of Early Earth's Atmosphere, Hydrosphere, and Biosphere—Constraints from Ore Deposits. In: Geological Society of America Memoir, vol. 198, pp. 81–104.

Kipp, A.M., Stëuken, E.E., Yun, M., Bekker, A., Buick, R., 2018. Pervasive aerobic nitrogen cycling in the surface ocean across the Paleoproterozoic Era. Earth Planet. Sci. Lett. 500, 117–126.

Kipp, M.A., Stüeken, E.E., Bekker, A., Buick, R., 2017. Selenium isotopes record extensive marine suboxia during the Great Oxidation Event. Proc. Natl. Acad. Sci. USA 114, 875–880.

Konhauser, K.O., et al., 2011. Aerobic bacterial pyrite oxidation and acid rock drainage during the Great Oxidation Event. Nature 478, 369–373.

König, S., et al., 2019. Redox induced sulfur-selenium isotope decoupling recorded in pyrite. Geochim. Cosmochim. Acta 244, 24–39.

Kump, L.R., et al., 2011. Isotopic Evidence for Massive Oxidation of Organic Matter Following the Great Oxidation Event. Science 334, 1694–1696.

Kurzawa, T., et al., 2017. A method for Se isotope analysis of low ng-level geological samples via double spike and hydride generation MC-ICP-MS. Chem. Geol. 466, 219–228.

Lam, P., Kuypers, M.M., 2011. Microbial nitrogen cycling processes in oxygen minimum zones. Annu. Rev. Mar. Sci. 3, 317–345.

Lenton, T.M., et al., 2014. Co-evolution of eukaryotes and ocean oxygenation in the Neoproterozoic era. Nat. Geosci. 7, 257–265.

Luo, J., et al., 2021. Pulsed oxygenation events drove progressive oxygenation of the early Mesoproterozoic ocean. Earth Planet. Sci. Lett. 559, 116754.

Lyons, T.W., Reinhard, C.T., Planavsky, N.J., 2014. The rise of oxygen in the Earth's early ocean and atmosphere. Nature 506, 307–315.

Mänd, K., et al., 2020. Palaeoproterozoic oxygenated oceans following the Lomagundi–Jatuli Event. Nat. Geosci. 13, 302–306.

Mänd, K., et al., 2022. Chromium evidence for protracted oxygenation during the Paleoproterozoic. Earth Planet. Sci. Lett. 584, 117501.

Marty, B., Zimmermann, L., Pujol, M., Burgess, R., Philippot, P., 2013. Nitrogen isotopic composition and density of the Archean atmosphere. Science 342, 101–104.

Miletto, M., Wang, X., Planavsky, N.J., Luther, G.W., Lyons, T.W., Tebo, B.M., 2021. Marine microbial Mn(II) oxidation mediates Cr(III) oxidation and isotope fractionation. Geochim. Cosmochim. Acta 297, 101–119.

Mitchell, K., et al., 2016. Geological evolution of the marine selenium cycle: insights from the bulk shale $\delta^{82/76}Se$ record and isotope mass balance modelling. Earth Planet. Sci. Lett. 441, 178–187.

Ossa Ossa, F., et al., 2013. Exceptional preservation of expandable clay minerals in the ca. 2.1 Ga black shales of the Francevillian basin, Gabon and its implication for atmospheric oxygen accumulation. Chem. Geol. 362, 181–192.

Ossa Ossa, F., et al., 2018. Two-step deoxygenation at the end of the Paleoproterozoic Lomagundi Event. Earth Planet. Sci. Lett. 486, 70–83.

Ossa Ossa, F., et al., 2019. Limited oxygen production in the Mesoarchean ocean. Proc. Natl. Acad. Sci. USA 116, 6647–6652.

Ossa Ossa, F., et al., 2021a. Limited expression of the Paleoproterozoic Oklo natural nuclear reactor phenomenon in the aftermath of a widespread deoxygenation event∼ 2.11–2.06 billion years ago. Chem. Geol. 558, 120315.

Ossa Ossa, F., König, S., Hofmann, A., Bekker, A., Spangenberg, J.E., Schoenberg, R., 2021b. Increase in ecosystem complexity aided organic carbon sequestration during the c. 2.22-2.06 Ga Lomagundi carbon isotope excursion. In: 23rd EGU General Assembly, held online 19–30 April 2021.

Planavsky, N.J., et al., 2011. Widespread iron-rich conditions in the mid-Proterozoic ocean. Nature 477, 448–451.
Planavsky, N.J., Bekker, A., Hofmann, A., Owens, J.D., Lyons, T.W., 2012. Sulfur record of rising and falling marine oxygen and sulfate levels during the Lomagundi event. Proc. Natl. Acad. Sci. USA 109, 18300–18305.
Planavsky, N.J., et al., 2014. Low Mid-Proterozoic atmospheric oxygen levels and the delayed rise of animals. Science 346, 635–638.
Poulton, S.W., Canfield, D.E., 2005. Development of a sequential extraction procedure for iron: implications for iron partitioning in continentally derived particulates. Chem. Geol. 214, 209–221.
Poulton, S.W., Canfield, D.E., 2011. Ferruginous conditions: a dominant feature of the ocean through Earth's history. Elements 7, 107–112.
Poulton, S.W., Fralick, P.W., Canfield, D.E., 2010. Spatial variability in oceanic redox structure 1.8 billion years ago. Nat. Geosci. 3, 486–490.
Poulton, S.W., Bekker, A., Cumming, V.M., Zerkle, A.L., Canfield, D.E., Johnston, D.T., 2021. A 200 million year delay in permanent atmospheric oxygenation. Nature 592, 232–236.
Préat, A., Bouton, P., Thiéblemont, D., Prian, J.P., Ndounze, S.S., Delpomdor, F., 2011. Paleoproterozoic high δ^{13}C dolomites from the Lastoursville and Franceville basins (SE Gabon): stratigraphic and synsedimentary subsidence implications. Precambrian Res. 189, 212–228.
Rudnick, R.L., Gao, S., 2014. Composition of Continental Crust. In: Holland, H.D., Turekian, K.K. (Eds.), Treatise on Geochemistry 4, 1–51.
Rue, E.L., Smith, G.J., Cutter, G.A., Bruland, K.W., 1997. The response of trace element redox couples to suboxic conditions in the water column. Deep-Sea Res. Part I 44, 113–134.
Sano, Y., Pillinger, C.T., 1990. Nitrogen isotopes and N2/Ar ratios in cherts: an attempt to measure time evolution of atmospheric δ15N value. Geochem. J. 24, 315–324.
Scott, C., et al., 2008. Tracing the stepwise oxygenation of the Proterozoic ocean. Nature 452, 456–459.
Scott, C., et al., 2014. Pyrite multiple-sulfur isotope evidence for rapid expansion and contraction of the early Paleoproterozoic seawater sulfate reservoir. Earth Planet. Sci. Lett. 389, 95–104.
Sigman, D.M., Fripiat, F., 2019. Nitrogen isotope in the ocean. In: Encyclopedia of Ocean Sciences, 3rd edition, vol. 1, pp. 263–278.
Stüeken, E.E., 2017. Selenium isotopes as a biogeochemical proxy in deep time. Rev. Mineral. Geochem. 82, 657–682.
Stüeken, E.E., et al., 2015. The evolution of the global selenium cycle: secular trends in Se isotopes and abundances. Geochim. Cosmochim. Acta 162, 109–125.
Stüeken, E.E., Kipp, M.A., Koehler, M.C., Buick, R., 2016. The evolution of Earth's biogeochemical nitrogen cycle. Earth-Sci. Rev. 160, 220–239.
Stüeken, E.E., Kuznetsov, A.B., Vasilyeva, I.M., Krupenin, M.T., Bekker, A., 2021. Transient deep-water oxygenation recorded by rare Mesoproterozoic phosphorites, South Urals. Precambrian Res. 360, 106242.
Stumm, W., Morgan, J.J., 1970. Aquatic Chemistry: An Introduction Emphasizing Chemical Equilibria in Natural Waters. Wiley-Interscience, New York, 583 pp.
von Strandmann, P.A.P., et al., 2015. Selenium isotope evidence for progressive oxidation of the Neoproterozoic biosphere. Nat. Commun. 6, 10157.
Warke, M.R., et al., 2020. The Great Oxidation Event preceded a Paleoproterozoic "snowball Earth". Proc. Natl. Acad. Sci. USA 117, 13314–13320.
Weber, F., 1968. Une série précambrienne du Gabon: le Francevillien. Sédimentologie, géochimie et relation avec les gîtes minéraux associés. Mém. Serv. Carte Géol. Als. Lorr. 28, 328 pp.
Zerkle, A.L., et al., 2017. Onset of the aerobic nitrogen cycle during the Great Oxidation Event. Nature 543, 465–467.
Zhang, K., Zhu, X., Wood, R.A., Shi, Y., Gao, Z., Poulton, S.W., 2018. Oxygenation of the Mesoproterozoic ocean and the evolution of complex eukaryotes. Nat. Geosci. 11, 345–350.
Zhang, X., Sigman, D.M., Morel, F.M., Kraepiel, A.M., 2014. Nitrogen isotope fractionation by alternative nitrogenases and past ocean anoxia. Proc. Natl. Acad. Sci. USA 111, 4782–4787.